Heliyon 10 (2024) e38718

Contents lists available at ScienceDirect

Heliyon

journal homepage: www.cell.com/heliyon

Research article

Mandatory role of endoplasmic reticulum in preserving NADPH regeneration in starved MDA-MB-231 breast cancer cells

Sonia Carta [a,*], Vanessa Cossu [b], Francesca Vitale [a], Matteo Bauckneht [a,c], Maddalena Ghelardoni [a], Anna Maria Orengo [a], Serena Losacco [a], Daniela Gaglio [d], Silvia Bruno [b], Sabrina Chiesa [a], Silvia Ravera [b], Gianmario Sambuceti [a,c], Cecilia Marini [a,d]

[a] IRCCS Ospedale Policlinico San Martino, 16132, Genova, Italy
[b] Department of Experimental Medicine, Human Anatomy Section, University of Genoa, 16132, Genova, Italy
[c] Department of Health Sciences, University of Genoa, 16132, Genova, Italy
[d] Institute of Molecular Bioimaging and Complex Biological Systems (IBSBC-CNR), National Research Council (CNR), 20054, Milan, Italy

ARTICLE INFO

Keywords:
Triple negative breast cancer
Glucose metabolism
NADPH
G6PD
H6PD
Pentose phosphate pathway
Redox stress

ABSTRACT

Cancer growth requires high amount of nicotinamide adenine dinucleotide phosphate (NADPH) to feed the anabolic reactions and preserve the redox balance. NADPH level is largely preserved by the oxidative arm of the pentose phosphate pathway (PPP). Here, we show that prolonged glucose deprivation of triple negative breast cancer MDA-MB-231 cells decreases proliferation rate, promotes hexose funneling to glycolysis hampering the PPP. The impairment in PPP activity and the consequent NADPH depletion are partially counterbalanced by enhancing the malic enzyme-1 catalyzed conversion of glutamine-derived malate to pyruvate. However, the use of these glucose-independent carbons implies the integrity of the two PPPs represented in all eukaryotic cells, i.e., the well-recognized cytosolic PPP, triggered by glucose-6-phosphate dehydrogenase (G6PD) and its reticular counterpart, triggered by hexose-6P-dehydrogenase (H6PD). This evidence configures the reticular PPP as a mandatory player in the regeneration of NADPH reductive power by cancer cells.

1. Introduction

The metabolic hallmark of cancer is a shift towards lactate fermentation despite normal oxygen tension [1,2]. The high ATP requirement associated with cell proliferation combined with the low efficiency of this "Warburg effect" implies a high glycolytic flux [3] and could therefore limit the availability of hexose to the pentose phosphate pathway (PPP), especially in the harsh tumor microenvironment.

Nevertheless, the high proliferation rate of cancer cells implies a high demand of NADPH levels for bio-reductive synthesis of nucleic acids and cell membranes [4]. Indeed, the reduction of ribonucleotides to deoxyribonucleotides requires 0.1 pmol NADPH/cell per division [4,5]. Similarly, the synthesis of one molecule of palmitic acid (the main component of cell membranes) requires 14 NADPH and only 7 ATP. The same NADPH is the main determinant of glutathione-dependent pathways that regulate intracellular

* Corresponding author.
E-mail address: sonia.carta@hsanmartino.it (S. Carta).

https://doi.org/10.1016/j.heliyon.2024.e38718
Received 30 September 2023; Received in revised form 19 September 2024; Accepted 27 September 2024
Available online 28 September 2024

redox status to prevent the activation of apoptotic pathways induced by the production of reactive oxygen species (ROS), which are typical of proliferating cells [6]. Accordingly, PPP is a crucial regulator of cancer cell proliferation, being both the main supplier of NADPH reducing power and virtually the only generator of ribose-5P required for nucleic acid synthesis [6,7]. In this study, we therefore wanted to test whether prolonged glucose deprivation is followed by a different response of glycolysis and PPP in the triple negative breast cancer cell line MDA-MB-231. In addition to well-recognized cytosolic arm triggered by glucose-6P-dehydrogenase (G6PD), we extended our investigation to another PPP confined within the endoplasmic reticulum (ER) and triggered by hexose-6-phosphate dehydrogenase (H6PD) [8], whose function in the capacity of cancer cells to proliferate and migrate has been documented by various laboratories [9–11].

2. Methods

2.1. Cell culture

MDA-MB-231 cells were obtained from ATCC (LGC Standards Srl, Milan, Italy) and cultured in Dulbecco's Modified Eagle Medium (DMEM, Gibco, Los Angeles, CA USA) with 10 % FBS, 25 mM glucose, 2 mM glutamine, 1 mM pyruvate, 1 % penicillin-streptomycin (Gibco, Grand Island, NY, USA), at 37 °C with 5 % CO_2. Experiments were performed in DMEM medium (plus all other above supplementations) with 25 mM glucose (control, HG) or only 2.5 mM glucose (LG). After 48 h, cells were harvested for the analysis.

2.2. Cell viability, cell culture growth and cell cycle analysis

Trypan blue-negative cells were counted to measure the cell growth. Cells were stained with 1 μg/ml propidium iodide (PI) (Enzo Life Sciences) and analyzed by FACScan Flow Cytometer (Becton Dickinson, Milan, Italy) to evaluate viability. Flow-cytometric measurements of DNA content were performed for cell cycle analysis. Cells were permeabilized with 0.05 % Triton X-100, stained 20 min with 30 μg/ml PI plus 0.5 mg/ml RNase, and measured on a FACSCalibur flow cytometer (BD Biosciences, San Diego, CA). Histograms of DNA content in at least 10 thousand cells provided by the same instrument were used to estimate cell cycle phase distribution. For all analyses, we used the FlowJo software (Version 10.8.1, Becton-Dickinson). Supplementary Fig. 1 reports representative gating images of flow cytometry analysis.

2.3. Seahorse analysis

Seahorse XFp Extracellular Flux Analyzer (Agilent Technologies) was used to determine the oxygen consumption rate (OCR) and extracellular acidification rate (ECAR). Cells (4,000 cells/well in XFp plates) were cultured in HG medium; after their adhesion, the medium was replaced with either HG or LG medium for 48 h. Thereafter Seahorse evaluation was performed according to the manufacturer's instructions. OCR and ECAR were measured both at baseline and following injections of the ATP-synthase inhibitor Oligomycin A (1.5 μM), the ATP synthesis uncoupler carbonyl cyanide-4-trifluoromethoxyphenylhydrazone (FCCP, 1.25 μM) and the Complex I + Complex III inhibitors (rotenone + antimycin A, 0.5 μM). Normalization for cell number was performed by crystal violet staining [12].

Proton efflux rate (PER) was calculated with WAVE software (Version 2.4, Agilent) using ECAR data and the buffer factor of HG and LG DMEM. PER value (picomol H^+x min^{-1}/million cells) was transformed in nanomoles of glucose used through glycolysis (nanomoles x min^{-1}/million cells) by the equation: Glucose + 2 ADP + 2 Pi → 2 Lactate + 2 ATP + $2H_2O$ + 2 H^+.

2.4. Enzymatic assays

NADP/NADPH ratio and total antioxidant capacity were assessed by a dedicated Kits (ab65349, Abcam, Cambridge, UK and MAK187, Sigma, St. Louis, MO, USA), following the manufacturer's instructions. Thiobarbituric acid reactive substances assay was used to evaluate Malondialdehyde levels [11,13]. Normalization was performed for the total protein concentrations.

2.5. Spectrophotometric assays

Spectrophometric assays were used to quantify the levels of glucose, lactate, pyruvate, ATP and LDH activity in cell lysates (20 μg) and lactate released in the supernatants. The samples were analyzed following the reduction of NADP (glucose and ATP) and NAD+ (lactate and pyruvate) or NADH oxidation (LDH) at 340 nm. Following solutions were used: Tris-HCl pH7.4 100 mM, MgCl2 0.2 mM, ATP 2 mM, purified hexokinase plus G6PD (Sigma-Aldrich) (glucose assay); Tris-HCl-pH7.4 100 mM, NAD+ 5 mM, 4 IU of LDH (Sigma-Aldrich) (lactate detection) [14]; Tris-HCl pH7.4 100 mM, pyruvate 5 mM and NAD+ 0.2 mM (LDH activity) [13]; 50 mM Tris HCl pH 8.0, 1 mM NADP, 10 mM MgCl2, and 5 mM glucose before and after the addition of 4 μg of purified hexokinase and G6PD (ATP quantification) [15]. Samples were analyzed spectrophotometrically at 340 nm and were normalized based on total protein content [14].

2.6. Western blot analysis

Cells were lysed in RIPA buffer with protease inhibitors. Western blotting was performed as described previously [14] and the

following antibodies were used: anti-H6PD (#ab170895, Abcam, Cambridge, UK), anti-G6PD (#ab124738, Abcam, Cambridge, UK), anti-MCT1 (#76508S, Cell Signaling Technology, Danvers, MA, USA), anti-phospho-PFKFB3 (Ser461) (#PA5-114619, Thermo Fisher Scientific, Waltham, MA, USA), anti- PFKFB3 (#MA5-32766, Thermo Fisher Scientific, Waltham, MA, USA), and anti-β-actin (#15G5A11/E2, Thermo Fisher Scientific, Waltham, MO, USA) or GAPDH (Novus biologicals, Bio-Techne, Minneapolis, USA) as the loading control. HRP–conjugated secondary antibodies were employed (Sigma-Aldrich, St. Louis, USA, 1:10,000 in PBS +0.15 % tween) and developed by an enhanced chemiluminescence substrate (ECL, Bio-Rad, Hercules, USA). Chemiluminescence system (Alliance 6.7 WL 20M, UVITEC, Cambridge, UK) and UV1D software (UVITEC, Cambridge, UK) were used for detection and analysis.

2.7. Transfection assay

Cells were transfected with 30 pmol siRNA and 9 μL Lipofectamine RNAiMAX (Thermo Fisher Scientific) in 6-well plates (200.000 cells/well). G6PD-siRNA (Silencer Select ID s5447, Thermo Fisher Scientific), H6PD-siRNA (Silencer ID s97551, Thermo Fisher Scientific) or Silencer Select Negative Control #2-siRNA (Thermo Fisher Scientific) were used. After 24 h the cells were reseeded in 24 well plates or Seahorse XFp plates and incubated 24 h in the same conditioned medium.

2.8. Real-time polymerase chain reaction

Total RNA was isolated with Quick RNA Miniprep Plus kit (Zymo Research) and cDNA synthesis was performed using SensiFAST

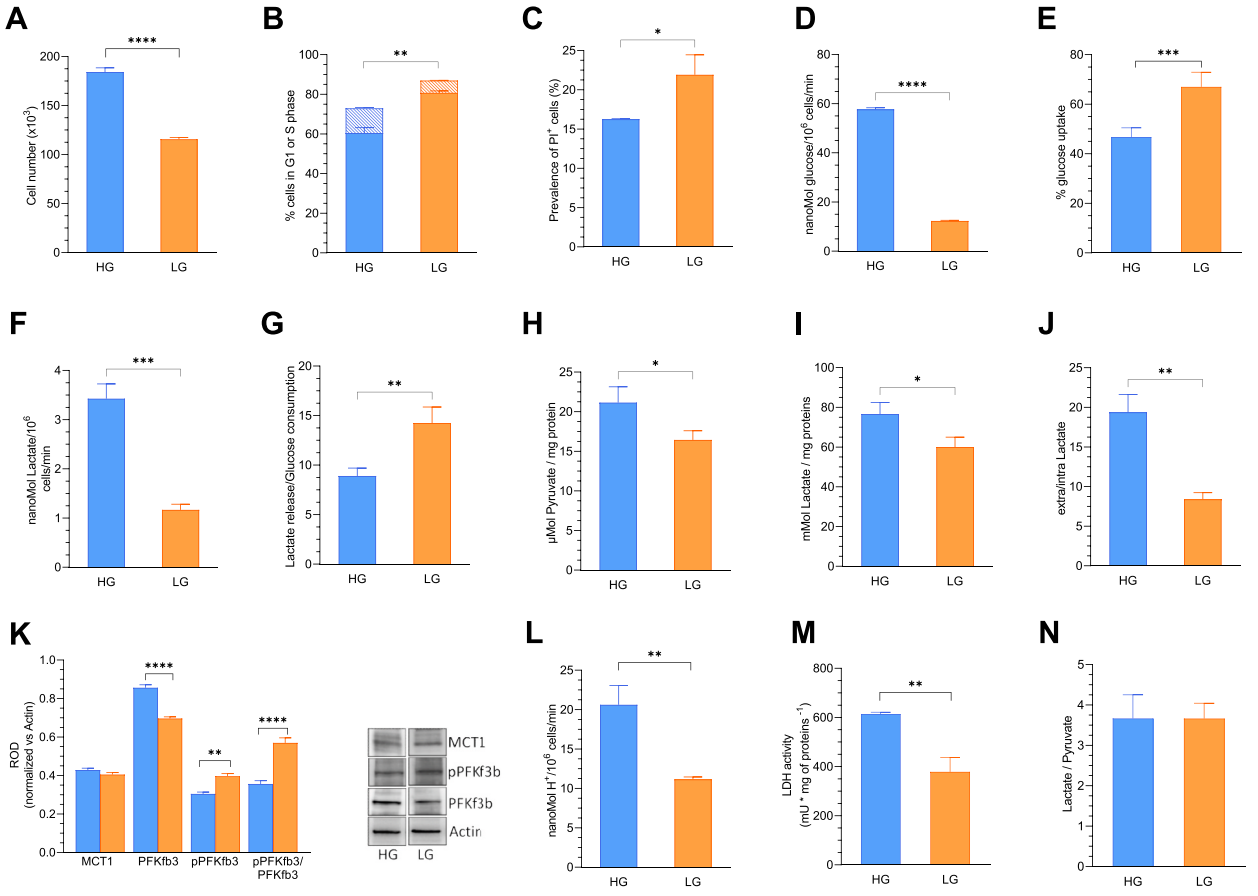

Fig. 1. Proliferation rate and metabolic response to glucose depletion. (A) Cell numbers of MDA-MB-231in HG (blue) or LG (orange) medium (n = 3). (B) Percent of cell cycle phase in HG (blue) or LG (orange) medium: G1 phase (empty column), S phase (dashed column) (n = 3). (C) Percent of PI^+ cells in MDA-MB-231cultured under HG (blue) or LG (orange) condition. (D and E) Medium glucose concentration (n = 3) (D) and % of glucose uptake (n = 3) (E) in HG and LG cultures after 48 h incubation. (F–J) Lactate release (n = 3) (F), lactate release/glucose consumption ratio (n = 3) (G), intracellular pyruvate (n = 3) (H), lactate content (n = 3) (I) and extra/intra lactate ratio (n = 3) (J) in MDA-MB-231 cultured in HG (blue) or LG (orange) medium. (K) Densitometric analyses (left) and a representative Western blot (right) of MCT1, PFKfb3 and pPFKfb3 normalized versus β-Actin in HG or LG medium (n = 3). (L) Instantaneous glycolytic flux of HG (blue) or LG (orange) cultures. (M and N) LDH activity (n = 3) (M) and ratio between lactate and pyruvate (n = 3) (N) under HG (blue) or LG (orange) condition. Data are represented as mean ± SD. * = $p < 0.05$; ** = $p < 0.01$; *** = $p < 0.001$; **** = $p < 0.0001$. (For interpretation of the references to colour in this figure legend, the reader is referred to the Web version of this article.)

cDNA Synthesis KIT (Bioline, Aurogene). G6PD, H6PD and ME1 genes were quantified in RT-PCR using Sensi FAST SYBR (Bioline). Gene expressions were analyzed with Q-Gene program and normalized to hypoxanthine-guanine phosophoribosyltransferase (HPRT) [16]. Specific primers designed by PRIMER 3 software and purchased from TIB MOLBIOL (Genoa, Italy) were used: G6PD: forward 5′-GGCAACAGATACAAGAACGTGA -3′, reverse 5′-GCCTCGGCTGCCATAAAT -3′; H6PD: forward 5′-GGACCATTACTTAGGCAAGCAG-3′ reverse 5′-CAGCATCCACGGTCTCTTTC-3′; ME 1: forward 5′ GGATTGCACACCTGATTGTG-3′ reverse 5′-TCTTCATGTTCATGGGCAAA-3′; HPRT: forward 5′CCTGGCGTCGTGATTAGTG-3′, reverse 5′-ACACCCTTTCCAAATCCTCAG-3′.

2.9. Metabolites extraction

MDA-MB-231 cells were seeded in 6well plates, washed with NaCl 0.9 % followed by 500 μl of ice-cold 70:30 acetonitrile:water. Cells were put 10min at −80 °C, collected by scraping and sonicated 5 s for 5 pulses at 70 % power twice. Cell lysate was centrifuged at 12000g for 10 min and supernatant was collected in a glass insert and dried in a centrifugal vacuum concentrator (Concentrator plus/ Vacufuge plus, Eppendorf) at 30 °C for 2.5 h. Before analysis, 150 μl of H_2O was added to the samples.

2.10. Liquid chromatography with tandem mass spectrometry metabolic profiling

The Agilent 1290 Infinity Ultra High Performance LC (UHPLC) system, along with an InfintyLab Poroshell 120 PFP column (2.1 × 100 mm, 2.7 μm; Agilent Technologies), were utilized in liquid chromatography with tandem mass spectrometry (LC-MS). The system was completed with an electrospray Dual JetStream source that operated in negative mode and a quadrupole-time of flight hybrid mass spectrometer (Agilent 6550 iFunnel Q-TOF). The MassHunter ProFinder (Agilent) was utilized to analyze and perform isotopic natural abundance correction on the data, which were normalized based on protein content. The data were obtained from *m/z* 60–1050 [17].

2.11. Statistical analysis

The data, derived from at least three independent experiments, are displayed as mean ± SD. When there were only two conditions being tested, the *t*-test was used for statistical analysis; otherwise, one-way analysis of variance (ANOVA) was used, and the multiple

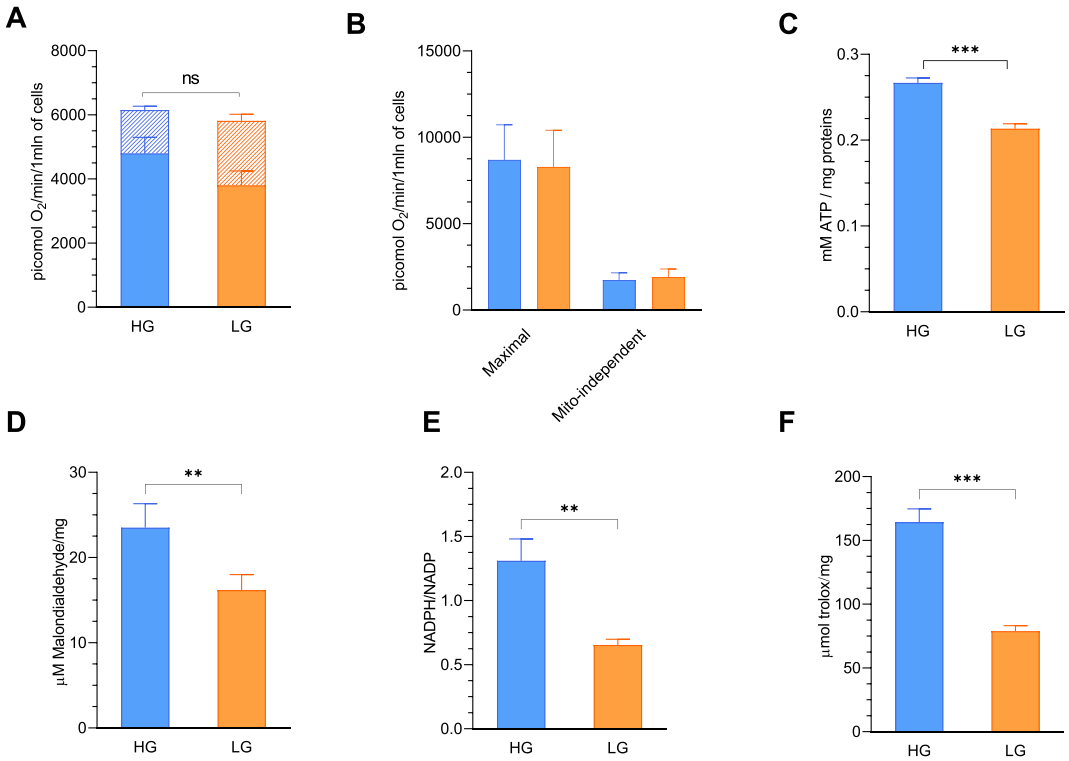

Fig. 2. Effect of partial glucose depletion on Oxygen usage, energy asset and redox stress. (A) Total OCR in MDA-MB-231 cells under HG (blue) or LG (orange) condition: ATP-dependent (empty column) and -independent (dashed column) OCR (n = 3). (B) Maximal and mitochondrial (Mito)-independent OCR under HG (blue) or LG (orange) condition (n = 3). (C–F) ATP intracellular concentration (n = 3) (C), malondialdehyde levels (n = 4) (D), NADPH/NADP ratio (n = 3) (E) and total antioxidant capacity (n = 3) (trolox, F) in HG (blue) or LG (orange) condition. Data are represented as mean ± SD. ** = $p < 0.01$; *** = $p < 0.001$; **** = $p < 0.0001$. (For interpretation of the references to colour in this figure legend, the reader is referred to the Web version of this article.)

comparison tool was used to find significant differences across all conditions. GraphPad Prism 9 were used for statistical analyses (GraphPad, San Diego, CA, USA) and p values < 0.05 was considered statistically significant.

3. Results

3.1. Metabolic reprogramming under glucose depletion

Glucose deprivation slowed down culture growth (Fig. 1A), G1-S transition (Fig. 1B) and impaired cell survival (Fig. 1C). The tenfold reduction of hexose availability (from 25 to 2.5 mM) decreased the amount of glucose removed from the incubation medium – and thus glucose consumption –approximately fivefold [to 21 % of HG cultures, Fig. 1D]. However, starved cells increased their glucose avidity, since the percentual amount of hexose removed from the medium (extraction fraction) increased of 20 % with respect to HG cultures (Fig. 1E). Lactate release slowed down to an even lesser degree (35 %) (Fig. 1F). Consequently, the net ratio between released lactate and consumed glucose boosted (>60 %) during starvation (Fig. 1G). This finding was not caused by an increased loss of the terminal glycolysis product. Indeed, despite the fivefold drop in glucose uptake, the intracellular levels of both pyruvate and lactate were only slightly decreased in LG with respect to HG cultures (Fig. 1H and I). Therefore, glucose deprivation almost halved the ratio between extra- and intra-cellular lactate concentration (Fig. 1J) despite the invariant abundance of monocarboxylate transporter 1 (MCT1) (Fig. 1K, and Supplementary Fig. 2A) as a possible index of a preserved metabolite transport across cell membrane [18].

Since the readout of this evaluation might have been contaminated by the different growth rates of HG and LG cultures during the 48 h of experiment, we assessed the instantaneous glycolytic flux using the Seahorse technology. The normalized proton efflux rate of LG cultures was even more preserved with respect to the biochemical assay and indicated an only halved lactate release despite the tenfold decrease in glucose availability (Fig. 1L).

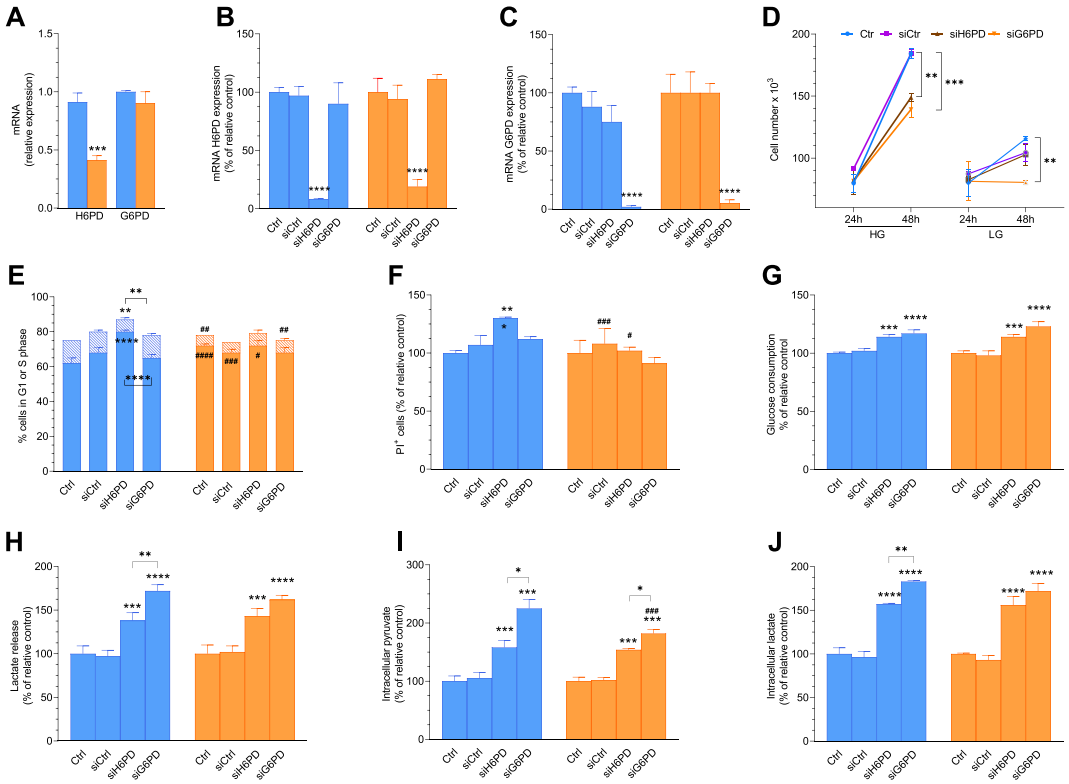

Fig. 3. Role of PPP in cell under glucose shortage. (A) H6PD and G6PD mRNA expression in MDA-MB-231grown under HG (blue) or LG (orange) condition (n = 3). (B and C) H6PD (B) and G6PD (C) mRNA expression under control (Ctrl), control siRNA (siCtrl), siRNA H6PD (siH6PD) or siRNA G6PD (siG6PD) in HG (blue) or LG (orange) condition, expressed as percentual of relative control (n = 3). (D) Cell numbers at 24 and 48 h of HG (left) and LG (right) condition under control (Ctrl, blue), control siRNA (siCtrl, purple), siRNA H6PD (siH6PD, brown) or siRNA G6PD (siG6PD, orange) (n = 3). (E) Percent of cell in cell cycle phase in HG (blue) or LG (orange) medium: G1 phase (empty column) and S phase (dashed column) (n = 3). (F–J) Percent of PI positive cells (n = 4) (F), glucose consumption (n = 3) (G), lactate release (n = 3) (H), intracellular pyruvate (n = 3) (I) and intracellular lactate (n = 3) (J) in MDA-MB-231 cells silenced for H6PD and G6PD in all experimental conditions under HG (blue) or LG (orange) medium, expressed as percentual of relative control. Data are represented as mean ± SD. * = $p < 0.05$; ** = $p < 0.01$; *** = $p < 0.001$; **** = $p < 0.0001$ versus corresponding control when alone, or between H6PD and G6PD siRNA when combined with the comparison line. # = $p < 0.05$; ### = $p < 0.001$; #### = $p < 0.0001$ versus corresponding condition in HG cultures. (For interpretation of the references to colour in this figure legend, the reader is referred to the Web version of this article.)

Accordingly, input (glucose) and output (lactate) balance indicated that the metabolic response to glucose depletion was characterized by an apparently paradoxical increase in the hexose channeling to the aerobic glycolysis.

Interestingly, the total expression of the 6-phosphofructo-2-kinase/fructose-2,6-biphosphatase 3 (PFKfb3), an allosteric regulator of glycolysis, was decreased under LG condition (Fig. 1K, and Supplementary Fig. 2). Starved cells, however, had a higher ratio of its phosphorylated to total free form, suggesting an activation of glycolytic flux. These data were opposed to lactate dehydrogenase (LDH) (Fig. 1M), the decrease of whose catalytic function agreed with the stability of lactate/pyruvate ratio (Fig. 1N).

3.2. Oxygen usage, energy asset and redox stress

Hypothetically, the preferential glucose channeling to glycolysis could reflect a respiratory impairment directly caused by glucose shortage. Nevertheless, starvation did not significantly modify both ATP-dependent and -independent OCR (Fig. 2A), as well as maximal and non-mitochondrial oxygen usage (Fig. 2B). Obviously, the scarce glucose availability, combined with its incomplete degradation maximal and mitochondrion-independent to lactate and the invariant mitochondrial respiration eventually decreased the ATP level in LG cultures (Fig. 2C). Moreover, the prolonged hexose deprivation did not result in the expected oxidative damage, since malondialdehyde levels were lower in LG with respect to HG cultures (Fig. 2D). On the other hand, the decreased access of glucose-6P to PPP was robustly confirmed by the marked decrease of both NADPH/NADP ratio (Fig. 2E) and total antioxidant capacity (Fig. 2F) induced by the prolonged glucose shortage.

Thus, the observed oxidative phosphorylation (OXPHOS) invariance, combined with the preferential glucose channeling to lactate of starved cells, mismatched the common assumption considering a large dependence of Krebs cycle activity on the glucose-derived pyruvate.

3.3. The role of PPP in the metabolic response to glucose shortage

To explain the enhanced glucose channeling to lactate fermentation associated with a significant deceleration of proliferating activity, we hypothesized that the cell proliferation was not directly inhibited by the energy depletion and rather reflected the decreased availability of the mandatory cofactor for nucleic acids synthesis, cell membranes production and redox equilibrium, i.e., NADPH.

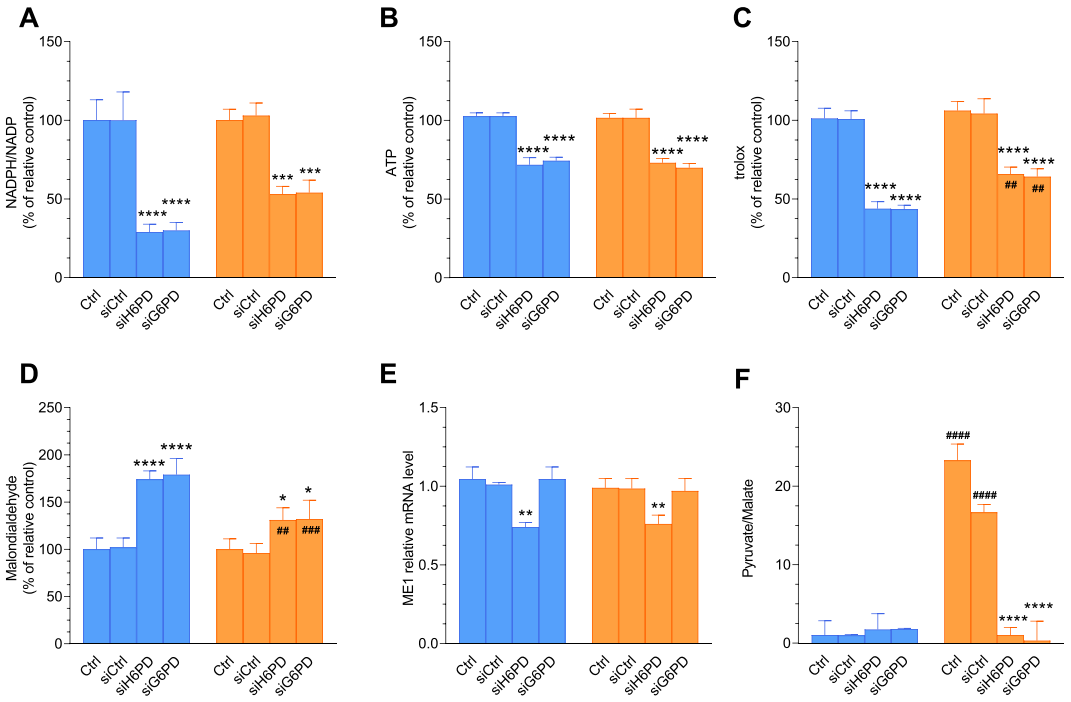

Fig. 4. Effect of H6PD and G6PD siRNA on energy asset, redox stress and NADPH regeneration. (A–D) NADPH/NADP ratio (n = 3) (A), ATP intracellular concentration (n = 3) (B), total antioxidant capacity (n = 3) (C) and malondialdehyde levels (n = 4) (D) under control (Ctrl), control siRNA (siCtrl), siRNA H6PD (siH6PD) or siRNA G6PD (siG6PD) in HG (blue) or LG (orange) medium, data are expressed as percentual of relative control. (E and F) mRNA ME1 expression (n = 3) (E) and Pyruvate/Malate ratio (n = 3) (F) under the same experimental conditions as A. Data are represented as mean ± SD. * = $p < 0.05$; ** = $p < 0.01$; *** = $p < 0.001$; **** = $p < 0.0001$ versus corresponding control. ## = $p < 0.001$; ### = $p < 0.001$; #### = $p < 0.0001$ versus corresponding condition in HG cultures. (For interpretation of the references to colour in this figure legend, the reader is referred to the Web version of this article.)

In order to confirm this theory, we estimated how the two PPP-triggering enzymes, G6PD and H6PD, were affected by a glucose shortage. At RT-PCR, starvation downregulated the gene expression of H6PD, while leaving unaltered the G6PD one (Fig. 3A). We thus verified the contribution of PPP in the metabolic response to glucose shortage evaluating the effect of both G6PD and H6PD gene silencing. Reproducing the Western Blot analysis (Supplementary Fig. 3), RT-PCR confirmed the effectiveness of siRNA and documented that downregulating either enzyme did not affect the expression of its counterpart, in agreement with previous studies [11] (Fig. 3B and C).

Overall, the downregulation of either PPP comparably decreased the growth of HG cultures. By contrast, it was less effective in LG ones whose growth was significantly inhibited only by G6PD silencing (Fig. 3D). G1-S transition was inhibited by H6PD silencing only in HG cultures, while LG ones were insensitive to the downregulation of both cytosolic and reticular PPP (Fig. 3E). The prevalence of PI positive cells was increased only by H6PD siRNA in HG cultures (Fig. 3F). Accordingly, these analyses indicated that proliferating activity of HG cultures required a preserved function of both reticular and cytosolic PPP as opposed to the LG ones that were more strictly dependent upon the function of the G6PD-triggered pathway.

This biological response was only partially reproduced by the metabolic pattern. Indeed, both G6PD and H6PD gene silencing significantly increased glucose consumption (Fig. 3G) and lactate release (Fig. 3H), regardless medium composition. On the other hand, both siRNAs markedly increased the cell content of both pyruvate and lactate with only a modest interference by the glucose shortage (Fig. 3I and J).

3.4. PPP control of glucose-independent NADPH regeneration

The NADPH/NADP ratio was decreased by the inhibition of cytosolic or reticular PPP to a comparable level in HG and LG cultures (Fig. 4A). A similar response characterized the energy asset (Fig. 4B) and the antioxidant capacity (Fig. 4C). By contrast, the worsening of oxidative damage induced by both siRNAs was partially prevented by starvation (Fig. 4D). This observation thus suggested that LG cultures activated pathways able to compensate the impairment in NADPH regeneration caused by the decreased PPP activity due to the combination of glucose shortage and its preferential channeling to glycolysis. In agreement with this concept, Murai and coworkers reported that starved cells largely utilize the reaction catalyzed by malic enzyme 1 (ME1) to regenerate the NADPH reductive power [19] through the NADP dependent decarboxylation of glutamate-derived malate to pyruvate [20].

ME1 gene expression was not affected by glucose shortage, while it was selectively inhibited by H6PD siRNA in both HG and LG conditions (Fig. 4E). We thus adopted a metabolomic approach to estimate the pyruvate/malate ratio. At this evaluation, the behavior of cell pyruvate content nicely reproduced the biochemical assay, showing an only slight decrease in LG cultures with respect to the HG ones (data not shown). By contrast, glucose shortage caused a profound depletion of malate leading to a >15fold increase of pyruvate/malate ratio (Fig. 4F). This striking response was virtually abolished by silencing either H6PD or G6PD (Fig. 4F) indicating a mandatory role for the simultaneous integrity of both cytosolic and reticular PPP to allow the response of ME1 catalyzed reaction to glucose shortage.

4. Discussion

In the present study, input/output analysis and instantaneous PER monitoring documented that decreasing glucose availability enhanced hexose channeling to glycolysis. The energy loss resulting from scarce fuel availability and its inefficient utilization did not accelerate OXPHOS despite preserved mitochondrial function. This behavior suggests that glucose metabolism in our model of triple-negative breast cancer cells is not only modulated by energy supply.

Combined with the metabolic response to G6PD and H6PD siRNA, this observation configures NADPH levels as a primary regulator of anabolic functions and thus of energy requirements in cancer. The present data extend the recognized importance of PPP as a primary promoter of cancer cell proliferation and survival [21] by showing that the integrity of the G6PD-triggered cytosolic pathway must be complemented by the activity of its reticular counterpart to ensure the regeneration of NADPH reductive power, even when provided by ME1 activity from glucose-independent sources.

4.1. Cooperation of cytosolic and reticular PPP in NADPH regeneration

Despite the apparent decrease in PPP activity caused by the combination of prolonged glucose shortage and its preferential channeling into glycolysis, LG cultures did not suffer from the oxidative damage typical of cells subjected to glucose deprivation [22]. By contrast, malondialdehyde levels were comparably increased by silencing either the G6PD or H6PD gene regardless of the composition of the medium. A similar response characterized the NADPH/NADP ratio. These data thus indicate that redox balance and NADPH levels cannot be preserved by the G6PD-triggered PPP alone and rather require the simultaneous function of the usually neglected reticular H6PD-triggered shunt.

Extensive literature previously documented that PPP is not the only source of NADPH-reducing power in cancer cells [6]. Folate-dependent one-carbon metabolism [23] is activated during high proliferative activity [24]. Similarly, starvation was found to accelerate the reaction catalyzed by ME1 [19], in contrast to isocitrate dehydrogenase-1, which accelerates NADP reduction only in the presence of high lactate concentration [20]. In the present study, prolonged glucose shortage markedly increased the pyruvate/malate ratio. This response would thus imply a metabolic shift able to regenerate NAPDH using other metabolites, most likely represented by the glutamine-derived produced in the mitochondria, transferred to the cytosol and thus converted to pyruvate by the NADP-dependent ME1-catalyzed reaction [25].

The role of glutaminolysis in cancer response to starvation has been already described [26]. Nevertheless, the present data first demonstrate the dependence of this metabolic shift on the simultaneous integrity of both G6PD- and H6PD-triggered PPPs. In other words, they configure the crosstalk between both oxidative arms and ME1 catalysis as a two-way communication system in which the role of ME1 in promoting the decarboxylation of 6P-gluconate to ribulose-5P [27] parallels the obligatory role of PPP activity in promoting the decarboxylative conversion of malate to pyruvate.

4.2. H6PD-triggered reticular PPP and starvation-induced cell death

The increased prevalence of PI + cells observed in H6PD-siRNA cultures extends the role of the reticular PPP in the preservation of cell viability during prolonged starvation. Jeon and coworkers [28] previously reported that 2-deoxyglucose (2DG) limited the incidence of induced cell death in starved cancer cells through mechanisms different from other glycolysis-inhibitor 5-thioglucose and associated with the appearance of 2-deoxygluconate-6P. Although in that study, this metabolite was considered the product of the G6PD-catalyzed reaction, this enzyme has been found unable to process both 2DG and 2DG-6P [9], which are instead substrates for H6PD. In agreement with this previous study, our data suggest the importance of reticular PPP in maintaining NADPH regeneration, either directly (with its oxidative arm) or indirectly (upregulating the expression of ME1), in the metabolic response to prolonged glucose deprivation, in contrast to the relatively low ineffectiveness of G6PD siRNA.

4.3. Limitations

The major limitation of the current study is that our findings are based on the in-vitro model of human triple-negative breast cancer. Therefore, more research is required to analyze the function of glucose and ER-PPP in different cancer cell lines or tumor organoid cultures, as a possibly more accurate model to mimic the characteristics of the original tumor.

As a second limitation, we did not attempt to selectively measure the NADPH/$NADP^+$ ratio in the cytosol and the ER lumen. This task is extremely complex in living cells and it has been only pursued in isolated microsomes [29]. Nevertheless, both HG and LG cultures showed a similar decrease in NADPH/$NADP^+$ ratio after either G6PD or H6PD silencing. Accordingly, these data confirm the relevant role of ER PPP in preserving the redox balance of the pyridine nucleotide of the selected cancer cells.

The awareness of the intense stress caused by the scarce glucose availability generated a wide literature evaluating the metabolic response of different cancer cells to glucose deprivation. Nevertheless, modeling the response of both glycolysis and PPP to glucose shortage is hampered by the wide variability of incubation time and medium content of other factors such as glutamine and fetal bovine serum (FBS). Here, the wide sets of evaluations were only applied to characterize lowering glucose concentration to levels close to those most likely encountered in vivo. This value was fixed at 2.5 mM because the chaotic vascularization coupled with the high rates of glucose consumption by the populating cells lower by 3–10 folds glucose availability in cancer with respect to normal tissues [30,31]. Moreover, the disordered nature of tumor microcirculation results in a heterogeneous nutrient distribution that, in the vital area of a breast tumor model, ranges from 1 to 5 μMol per gram of tissue (and thus approximately 1–5 mM) according to the distance from the closest capillary [32]. A detailed comprehension of MDA-MB-231 metabolic patterns would have implied drawing a concentration-response curve. However, even such a vast experimental protocol would have been severely flawed by the impossibility of accounting for signaling elicited by cells exposed to largely different glucose levels in a relatively small microenvironment.

5. Conclusion

Here we show that a prolonged incubation of MDA-MB-231 cancer cells to glucose levels close to those encountered in vivo enhances the hexose channeling to glycolysis. The consequent impairment in PPP activity does not result in significant oxidative damage, because of a missing acceleration of OXPHOS activity. Glucose shortage activates the ME1-catalyzed reaction, most likely utilizing glutamate-derived malate for the NADP-dependent decarboxylative conversion into pyruvate.

While the underlying mechanisms remain unclear, the current data show that the use of glucose-independent carbons for NADP reduction compulsorily asks for the integrity of both the recognized G6PD-triggered PPP in the cytosol and its counterpart confined within the endoplasmic reticulum. In other words, the hitherto unconsidered H6PD reproduces the G6PD role in allowing the regeneration of NADPH levels needed for the bio-reductive synthesis and the redox control of cancer cells.

Funding statement

This work was supported by the grant AIRC (code IG 23201), by the program Ricerca Corrente 2022–2024 and by project H2UB (code T4-AN-10) of the Italian Ministry of Health.

Data availability statement

Data will be made available on request.

Ethics statement

No ethic issue was approached by this study focused on in vitro cell cultures.

CRediT authorship contribution statement

Sonia Carta: Writing – original draft, Investigation, Formal analysis, Data curation, Conceptualization. **Vanessa Cossu:** Investigation, Formal analysis, Data curation, Conceptualization. **Francesca Vitale:** Methodology, Formal analysis, Data curation, Conceptualization. **Matteo Bauckneht:** Writing – review & editing, Visualization, Formal analysis. **Maddalena Ghelardoni:** Methodology, Formal analysis. **Anna Maria Orengo:** Writing – review & editing, Formal analysis. **Serena Losacco:** Methodology. **Daniela Gaglio:** Methodology. **Silvia Bruno:** Writing – original draft, Visualization, Methodology. **Sabrina Chiesa:** Writing – review & editing, Formal analysis. **Silvia Ravera:** Writing – review & editing, Methodology, Investigation. **Gianmario Sambuceti:** Writing – original draft, Validation, Supervision, Funding acquisition, Conceptualization. **Cecilia Marini:** Writing – original draft, Validation, Project administration, Formal analysis, Conceptualization.

Declaration of competing interest

The authors declare that they have no known competing financial interests or personal relationships that could have appeared to influence the work reported in this paper.

Appendix A. Supplementary data

Supplementary data to this article can be found online at https://doi.org/10.1016/j.heliyon.2024.e38718.

References

[1] O. Warburg, F. Wind, E. Negelein, The metabolism of tumors in the body, J. Gen. Physiol. 8 (1927) 519–530, https://doi.org/10.1085/jgp.8.6.519.
[2] O. Warburg, On respiratory impairment in cancer cells, Science 124 (1956) 269–270.
[3] M.G. Vander Heiden, L.C. Cantley, C.B. Thompson, Understanding the Warburg effect: the metabolic requirements of cell proliferation, Science 324 (2009) 1029–1033, https://doi.org/10.1126/science.1160809.
[4] L. Sun, C. Suo, S. Li, H. Zhang, P. Gao, Metabolic reprogramming for cancer cells and their microenvironment: beyond the Warburg Effect, Biochim. Biophys. Acta Rev. Canc 1870 (2018) 51–66, https://doi.org/10.1016/j.bbcan.2018.06.005.
[5] A.N. Lane, T.W. Fan, Regulation of mammalian nucleotide metabolism and biosynthesis, Nucleic Acids Res. 43 (2015) 2466–2485, https://doi.org/10.1093/nar/gkv047.
[6] H. Ju, J. Lin, T. Tian, D. Xie, R. Xu, NADPH homeostasis in cancer: functions, mechanisms and therapeutic implications, Signal Transduct. Targeted Ther. 5 (2020) 231, https://doi.org/10.1038/s41392-020-00326-0.
[7] P. Jiang, W. Du, M. Wu, Regulation of the pentose phosphate pathway in cancer, Protein Cell 5 (2014) 592–602, https://doi.org/10.1007/s13238-014-0082-8.
[8] S. Senesi, M. Csala, P. Marcolongo, R. Fulceri, J. Mandl, G. Banhegyi, A. Benedetti, Hexose-6-phosphate dehydrogenase in the endoplasmic reticulum, Biol. Chem. 391 (2010) 1–8, https://doi.org/10.1515/BC.2009.146.
[9] C. Marini, S. Ravera, A. Buschiazzo, G. Bianchi, A.M. Orengo, S. Bruno, G. Bottoni, L. Emionite, F. Pastorino, E. Monteverde, L. Garaboldi, R. Martella, B. Salani, D. Maggi, M. Ponzoni, F. Fais, L. Raffaghello, G. Sambuceti, Discovery of a novel glucose metabolism in cancer: the role of endoplasmic reticulum beyond glycolysis and pentose phosphate shunt, Sci. Rep. 6 (2016) 25092, https://doi.org/10.1038/srep25092.
[10] M. Tsachaki, N. Mladenovic, H. Stambergova, J. Birk, A. Odermatt, Hexose-6-phosphate dehydrogenase controls cancer cell proliferation and migration through pleiotropic effects on the unfolded-protein response, calcium homeostasis, and redox balance, Faseb. J. 32 (2018) 2690–2705, https://doi.org/10.1096/fj.201700870RR.
[11] V. Cossu, M. Bonanomi, M. Bauckneht, S. Ravera, N. Righi, A. Miceli, S. Morbelli, A.M. Orengo, P. Piccioli, S. Bruno, D. Gaglio, G. Sambuceti, C. Marini, Two high-rate pentose-phosphate pathways in cancer cells, Sci. Rep. 10 (2020) 22111–22112, https://doi.org/10.1038/s41598-020-79185-2.
[12] J. Nilles, J. Weiss, D. Theile, Crystal violet staining is a reliable alternative to bicinchoninic acid assay-based normalization, Biotechniques 73 (2022) 131–135, https://doi.org/10.2144/btn-2022-0064.
[13] C. Marini, V. Cossu, M. Bauckneht, S. Carta, F. Lanfranchi, F. D'Amico, S. Ravera, A.M. Orengo, C. Ghiggi, F. Ballerini, P. Durando, S. Chiesa, A. Miceli, M. I. Donegani, S. Morbelli, S. Bruno, G. Sambuceti, Mitochondrial generated redox stress differently affects the endoplasmic reticulum of circulating lymphocytes and monocytes in treatment-naive Hodgkin's lymphoma, Antioxidants 11 (2022) 762, https://doi.org/10.3390/antiox11040762, 10.3390/antiox11040762.
[14] V. Cossu, C. Marini, P. Piccioli, A. Rocchi, S. Bruno, A.M. Orengo, L. Emionite, M. Bauckneht, F. Grillo, S. Capitanio, E. Balza, N. Yosifov, P. Castellani, G. Caviglia, I. Panfoli, S. Morbelli, S. Ravera, F. Benfenati, G. Sambuceti, Obligatory role of endoplasmic reticulum in brain FDG uptake, Eur. J. Nucl. Med. Mol. Imag. 46 (2019) 1184–1196, https://doi.org/10.1007/s00259-018-4254-2.
[15] S. Ravera, M. Podesta, F. Sabatini, C. Fresia, M. Columbaro, S. Bruno, E. Fulcheri, L.A. Ramenghi, F. Frassoni, Mesenchymal stem cells from preterm to term newborns undergo a significant switch from anaerobic glycolysis to the oxidative phosphorylation, Cell. Mol. Life Sci. 75 (2018) 889–903, https://doi.org/10.1007/s00018-017-2665-z.
[16] P. Simon, Q-Gene: processing quantitative real-time RT-PCR data, Bioinformatics 19 (2003) 1439–1440, https://doi.org/10.1093/bioinformatics/btg157.
[17] C. Marini, V. Cossu, S. Carta, E. Greotti, D. Gaglio, N. Bertola, S. Chiesa, S. Bruno, F. Vitale, M. Bonanomi, D. Porro, M. Riondato, A.M. Orengo, M. Bauckneht, S. Morbelli, S. Ravera, G. Sambuceti, Fundamental role of pentose phosphate pathway within the endoplasmic reticulum in glutamine addiction of triple-negative breast cancer cells, Antioxidants 12 (2022) 43, https://doi.org/10.3390/antiox12010043, 10.3390/antiox12010043.
[18] A.P. Halestrap, M.C. Wilson, The monocarboxylate transporter family–role and regulation, IUBMB Life 64 (2012) 109–119, https://doi.org/10.1002/iub.572.
[19] S. Murai, A. Ando, S. Ebara, M. Hirayama, Y. Satomi, T. Hara, Inhibition of malic enzyme 1 disrupts cellular metabolism and leads to vulnerability in cancer cells in glucose-restricted conditions, Oncogenesis 6 (2017) e329, https://doi.org/10.1038/oncsis.2017.34.
[20] M. Ying, D. You, X. Zhu, L. Cai, S. Zeng, X. Hu, Lactate and glutamine support NADPH generation in cancer cells under glucose deprived conditions, Redox Biol. 46 (2021) 102065, https://doi.org/10.1016/j.redox.2021.102065.
[21] K.C. Patra, N. Hay, The pentose phosphate pathway and cancer, Trends Biochem. Sci. 39 (2014) 347–354, https://doi.org/10.1016/j.tibs.2014.06.005.
[22] D.R. Spitz, J.E. Sim, L.A. Ridnour, S.S. Galoforo, Y.J. Lee, Glucose deprivation-induced oxidative stress in human tumor cells. A fundamental defect in metabolism? Ann. N. Y. Acad. Sci. 899 (2000) 349–362, https://doi.org/10.1111/j.1749-6632.2000.tb06199.x.
[23] X. Liu, Y. Zhang, L. Zhuang, K. Olszewski, B. Gan, NADPH debt drives redox bankruptcy: SLC7A11/xCT-mediated cystine uptake as a double-edged sword in cellular redox regulation, Genes Dis 8 (2020) 731–745, https://doi.org/10.1016/j.gendis.2020.11.010.
[24] I. Ben-Sahra, G. Hoxhaj, S.J.H. Ricoult, J.M. Asara, B.D. Manning, mTORC1 induces purine synthesis through control of the mitochondrial tetrahydrofolate cycle, Science 351 (2016) 728–733, https://doi.org/10.1126/science.aad0489.

[25] R.J. DeBerardinis, A. Mancuso, E. Daikhin, I. Nissim, M. Yudkoff, S. Wehrli, C.B. Thompson, Beyond aerobic glycolysis: transformed cells can engage in glutamine metabolism that exceeds the requirement for protein and nucleotide synthesis, Proc. Natl. Acad. Sci. U. S. A. 104 (2007) 19345–19350, https://doi.org/10.1073/pnas.0709747104.
[26] T. Li, C. Copeland, A. Le, Glutamine metabolism in cancer, Adv. Exp. Med. Biol. 1311 (2021) 17–38, https://doi.org/10.1007/978-3-030-65768-0_2.
[27] P. Yao, H. Sun, C. Xu, T. Chen, B. Zou, P. Jiang, W. Du, Evidence for a direct cross-talk between malic enzyme and the pentose phosphate pathway via structural interactions, J. Biol. Chem. 292 (2017) 17113–17120, https://doi.org/10.1074/jbc.M117.810309.
[28] S. Jeon, N.S. Chandel, N. Hay, AMPK regulates NADPH homeostasis to promote tumour cell survival during energy stress, Nature 485 (2012) 661–665, https://doi.org/10.1038/nature11066.
[29] A.E. Zielinska, E.A. Walker, P.M. Stewart, G.G. Lavery, Biochemistry and physiology of hexose-6-phosphate knockout mice, Mol. Cell. Endocrinol. 336 (2011) 213–218, https://doi.org/10.1016/j.mce.2010.12.004.
[30] A. Hirayama, K. Kami, M. Sugimoto, M. Sugawara, N. Toki, H. Onozuka, T. Kinoshita, N. Saito, A. Ochiai, M. Tomita, H. Esumi, T. Soga, Quantitative metabolome profiling of colon and stomach cancer microenvironment by capillary electrophoresis time-of-flight mass spectrometry, Cancer Res. 69 (2009) 4918–4925, https://doi.org/10.1158/0008-5472.CAN-08-4806.
[31] K. Birsoy, R. Possemato, F.K. Lorbeer, E.C. Bayraktar, P. Thiru, B. Yucel, T. Wang, W.W. Chen, C.B. Clish, D.M. Sabatini, Metabolic determinants of cancer cell sensitivity to glucose limitation and biguanides, Nature 508 (2014) 108–112, https://doi.org/10.1038/nature13110.
[32] T. Schroeder, H. Yuan, B.L. Viglianti, C. Peltz, S. Asopa, Z. Vujaskovic, M.W. Dewhirst, Spatial heterogeneity and oxygen dependence of glucose consumption in R3230Ac and fibrosarcomas of the Fischer 344 rat, Cancer Res. 65 (2005) 5163–5171, https://doi.org/10.1158/0008-5472.CAN-04-3900.